Sb$_2$Te$_3$ Nanoparticles with Enhanced Seebeck Coefficient and Low Thermal Conductivity

Jing Chen,[†] Ting Sun,[†] DaoHao Sim,[†] Haiyang Peng,[‡] Huatao Wang,[‡]
Shufen Fan,[†] Huey Hoon Hng,[†] Jan Ma,[†] Freddy Yin Chang Boey,[†] Sean Li,[§]
Majid Kabiri Samani,[∥] George Chung Kit Chen,[∥] Xiaodong Chen,[†] Tom Wu,[‡] and Qingyu Yan*,[†]

[†]*School of Materials Science and Engineering, Nanyang Technological University, 50 Nanyang Avenue,
Singapore 639798, Singapore,* [‡]*Division of Physics and Applied Physics, School of Physical and
Mathematical Sciences, Nanyang Technological University, 50 Nanyang Avenue, Singapore 639798,
Singapore,* [§]*School of Materials Science and Engineering, University of New South Wales, NSW 2052,
Australia, and* [∥]*School of Electrical and Electronic Engineering, Nanyang Technological University,
Singapore 639798, Singapore*

Nanostructured thermoelectric semiconductors represent a promising new direction that can further increase energy conversion efficiency, which requires the realization of thermoelectric nanocrystals with size comparable to their de Broglie wavelength while maintaining a high electrical conductivity. Here, we demonstrate a new facile process to grow self-assembled Sb$_2$Te$_3$ nanoparticles with controlled particle size and enhanced thermoelectric properties by using a catalyst-free vapor transport growth technique. The samples show much more enhanced Seebeck coefficients than that of bulk Sb$_2$Te$_3$ with similar charge carrier concentration. Meanwhile, the thermal conductivity measurements with pulse photothermal reflectance suggest that the these Sb$_2$Te$_3$ nanoparticle films show much reduced thermal conductivity as compared to that of bulk Sb$_2$Te$_3$. The discussed approach is promising for realizing new types of highly efficient thermoelectric semiconductors.

Introduction

The realization of a high-efficiency thermoelectric (TE) module for solid state energy conversion requires the development of TE semiconductors with high figure of merit,[1] which is a dimensionless factor expressed as $ZT = (S^2\sigma/\kappa)T$, where T is the temperature in kelvins, S is the Seebeck coefficient, σ is the electrical conductivity and κ is the thermal conductivity. Among all the TE semiconductors, Sb$_2$Te$_3$ and their alloys have been extensively studied due to their promising ZT values in the temperature range of 300−500 K.[2−4] Further enhancement of ZT is expected by nanostructuring these semiconductors[5] due to the occurrence of quantum size effect leading to the enhancement of S[6,7] and increased interface scattering of phonons to reduce the thermal conductivity.[4,8−10]

Sb$_2$Te$_3$ nanostructures have been prepared by various methods including solvothermal,[11,12] electrochemical

*Address correspondence to this author. E-mail: alexyan@ntu.edu.sg.
(1) Tritt, T. M. Thermoelectric materials—Holey and unholey semiconductors. *Science* **1999,** *283*(5403), 804–805.
(2) Kim, T. S.; Chun, B. S.; Lee, J. K.; Jung, H. G. In *Thermoelectric properties of gas atomized p-type Sb2Te3−25% Bi2Te3 alloys*; 12th International Symposium on Metastable and Nano-Materials (ISMANAM-2005), Paris, France, July 03−07, 2005; pp 710−713.
(3) Venkatasubramanian, R.; Siivola, E.; Colpitts, T.; O'Quinn, B. Thin-film thermoelectric devices with high room-temperature figures of merit. *Nature* **2001,** *413*(6856), 597–602.
(4) Harman, T. C.; Taylor, P. J.; Walsh, M. P.; LaForge, B. E. Quantum dot superlattice thermoelectric materials and devices. *Science* **2002,** *297*(5590), 2229–2232.
(5) Dresselhaus, M. S.; Chen, G.; Tang, M. Y.; Yang, R. G.; Lee, H.; Wang, D. Z.; Ren, Z. F.; Fleurial, J. P.; Gogna, P. New directions for low-dimensional thermoelectric materials. *Adv. Mater.* **2007,** *19*(8), 1043–1053.
(6) Yan, Q. Y.; Chen, H.; Zhou, W. W.; Hng, H. H.; Boey, F. Y. C.; Ma, J. A Simple Chemical Approach for PbTe Nanowires with Enhanced Thermoelectric Properties. *Chem. Mater.* **2008,** *20*(20), 6298–6300.
(7) Wang, R. Y.; Feser, J. P.; Lee, J. S.; Talapin, D. V.; Segalman, R.; Majumdar, A. Enhanced thermopower in PbSe nanocrystal quantum dot superlattices. *Nano Lett.* **2008,** *8*(8), 2283–2288.
(8) Poudel, B.; Hao, Q.; Ma, Y.; Lan, Y. C.; Minnich, A.; Yu, B.; Yan, X.; Wang, D. Z.; Muto, A.; Vashaee, D.; Chen, X. Y.; Liu, J. M.; Dresselhaus, M. S.; Chen, G.; Ren, Z. High-thermoelectric performance of nanostructured bismuth antimony telluride bulk alloys. *Science* **2008,** *320*(5876), 634–638.
(9) Hsu, K. F.; Loo, S.; Guo, F.; Chen, W.; Dyck, J. S.; Uher, C.; Hogan, T.; Polychroniadis, E. K.; Kanatzidis, M. G. Cubic AgPbmSbTe2+m: Bulk thermoelectric materials with high figure of merit. *Science* **2004,** *303*(5659), 818–821.
(10) Hochbaum, A. I.; Chen, R. K.; Delgado, R. D.; Liang, W. J.; Garnett, E. C.; Najarian, M.; Majumdar, A.; Yang, P. D. Enhanced thermoelectric performance of rough silicon nanowires. *Nature* **2008,** *451*(7175), 163–U5.
(11) Wang, W. Z.; Poudel, B.; Yang, J.; Wang, D. Z.; Ren, Z. F. High-yield synthesis of single-crystalline antimony telluride hexagonal nanoplates using a solvothermal approach. *J. Am. Chem. Soc.* **2005,** *127*(40), 13792–13793.
(12) Groshens, T. J.; Gedridge, R. W.; Lowema, C. K. Room-temperature MOCVD of Sb$_2$Te$_3$ films and solution precipitation of M$_2$Te$_3$ (M = Sb, Bi) powders via a novel (*N,N*-dimethylamino)trimethylsilane elimination-reaction. *Chem. Mater.* **1994,** *6*(6), 727–729.
(13) Xiao, F.; Hangarter, C.; Yoo, B.; Rheem, Y.; Lee, K. H.; Myung, N. V. Recent progress in electrodeposition of thermoelectric thin films and nanostructures. *Electrochim. Acta* **2008,** *53*(28), 8103–8117.
(14) Meister, S.; Peng, H. L.; McIlwrath, K.; Jarausch, K.; Zhang, X. F.; Cui, Y. Synthesis and characterization of phase-change nanowires. *Nano Lett.* **2006,** *6*(7), 1514–1517.

deposition,[13] and catalyzed vapor−liquid−solid (VLS) growth.[14,15] These methods all have many advantages and some disadvantages. For example, solvothermal processes can easily produce nanocrystals with uniform size, shape and composition with possible scale-up production yield. But the shape and size control may require insulating capping ligands that need to be removed to achieve appropriate electrical conductivity. Electrochemical deposition can produce nanocrystals with predefined shape, size and uniformity. But it may require the removal of anodic aluminum oxide (AAO) templates. Catalyzed vapor−liquid−solid growth can deposit single crystalline nanowires with excellent control of structural orientation, size and aspect ratio. But the yield of the growth may not be high enough for thermoelectric module integration. Currently, the fabrication of nanocrystalline TE modules still largely depends on ball milling combined with hot pressing,[8] or nanostructuring of bulk materials,[16−18] which does not give adequate control over the crystal size, and excessive crystal growth is inevitable during the process.

In this study, we introduce the fabrication of assembled Sb_2Te_3 nanoparticle films by a simple vapor transport process without the assistance of any catalyst. The size of the Sb_2Te_3 particles can be tuned in the range of $10-100$ nm by varying the growth parameters, i.e., the Ar/H_2 flow rate and the substrate temperature/substrate position. The as-prepared assembled nanoparticle films show reduced electrical resistivity while high electrical resistivity is an important issue related to applications of TE nanocrystals prepared by wet-chemistry processes.[7,19] Meanwhile, these nanoparticle films show much enhanced Seebeck coefficients as compared to that of bulk Sb_2Te_3.[20,21] Furthermore, these Sb_2Te_3 nanoparticle films show much reduced thermal conductivity as compared to that of bulk Sb_2Te_3, which leads to an estimated maximum ZT value > 1.1 at 500 K for 20 nm particle films annealed at 523 K for 60 min. To our best knowledge, such close-packed nanoparticle films with controllable particle size by the simple vapor transport growth process have not been reported before. This growth process holds promising potential to produce assembled nanocrystal samples for nanoelectronics with good electrical conductivity (e.g., tedious chemical processes are not required to remove surface capping ligands as in the wet chemical processes[19,22,23]), defined nanoparticle/grain size and well-crystallized phases, which are keys to induce many performance enhancements.

Experimental Section

Synthesis of Sb_2Te_3 Nanoparticles. Te powder (Aldrich, 99.8%, 200 mesh) and Sb powder (Sigma-Aldrich, 99.5%, 100 mesh) were used as received. Glass slides (1.5×1 cm) were carefully washed by ethanol and DI water and then dried. The experiment was carried out in a horizontal tube furnace (Lindberg/Blue M). Sb powder was placed at the center of the tube furnace, and Te powder was placed at 15 cm upstream of the Sb powder. Ten pieces of glass substrates were placed at $20-30$ cm downstream of the Sb source. Before starting the growth process, the quartz tube was evacuated to 10^{-3} mbar and then flushed with 95% Ar + 5% H_2 gas 3 times to prevent possible oxidation of the samples. The furnace was heated to 853 K with a heating rate of 30 K/min and kept for 3 h. During the growth, the flow rate of 95% Ar + 5% H_2 gas was controlled at 200 sccm (standard cubic centimeters per minute) by a mass flow meter controller. The pressure in the quartz tube was kept at 2.6 mbar by regulating the pump speed of the mechanical pump.

Materials Characterization. The as-prepared and annealed Sb_2Te_3 nanoparticle films on glass substrates were directly used for SEM and XRD measurements. The X-ray diffractograms were obtained by using a Scintag PAD-V diffractometer with Cu Kα irradiation. The size and morphology of the particles were characterized using a field-emission SEM (JEOL JSM6340F) operating at 5 kV. For TEM characterization, the samples were put into a small ampule. Ethanol was then added until it covered the surface of the substrate. After ultrasonication for 2 h, the solution was drop cast onto carbon coated 200 mesh Cu grids. HRTEM and EDX were obtained by using a JEOL 2100 system operating at 200 kV. TEM and SAED measurements were carried out by using a JEOL 2010 system operating at 200 kV. The thickness of the film was measured using a scanning probe station and confirmed by the cross-section SEM.

Thermoelectric Properties Characterization. The resistivity and Seebeck coefficient were measured from 323 to 573 K using a commercially available ZEM 3 Seebeck meter under a helium environment. The thickness of the films, used to calculate the electric resistivity, was measured by a scanning probe station and confirmed by the cross-section SEM. The effective charge carrier concentration of samples was measured using a typical S7-500-1-0.55T probe station with Keithley 4200 semiconductor characterization, adjustable pole electromagnet (model 1607037) and hall effect gauss meter (model GM-700).

(15) Lee, J. S.; Brittman, S.; Yu, D.; Park, H. Vapor-liquid-solid. and vapor-solid growth of phase-change Sb_2Te_3 nanowires and Sb_2Te_3/GeTe nanowire heterostructures. *J. Am. Chem. Soc.* **2008**, *130*(19), 6252–6258.

(16) Sootsman, J. R.; Kong, H.; Uher, C.; D'Angelo, J. J.; Wu, C. I.; Hogan, T. P.; Caillat, T.; Kanatzidis, M. G. Large Enhancements in the Thermoelectric Power Factor of Bulk PbTe at High Temperature by Synergistic Nanostructuring. *Angew. Chem., Int. Ed.* **2008**, *47*(45), 8618–8622.

(17) Heremans, J. P.; Thrush, C. M.; Morelli, D. T., Thermopower enhancement in PbTe with Pb precipitates. J. Appl. Phys. **2005**, *98*(6), doi: 10.1063/1.2037209.

(18) Gorsse, S.; Pereira, P. B.; Decourt, R.; Sellier§, E. Microstructure Engineering Design for Thermoelectric Materials: An Approach to Minimize Thermal Diffusivity. *Chem. Mater.* **2010**, *22*, 988–993.

(19) Urban, J. J.; Talapin, D. V.; Shevchenko, E. V.; Kagan, C. R.; Murray, C. B. Synergismin binary nanocrystal superlattices leads to enhanced p-type conductivity in self-assembled PbTe/Ag-2 Te thin films. *Nat. Mater.* **2007**, *6*(2), 115–121.

(20) Drasar, C.; Steinhart, M.; Lost'ak, P.; Shin, H. K.; Dyck, J. S.; Uher, C. Transport coefficients of titanium-doped Sb2Te3 single crystals. *J. Solid State Chem.* **2005**, *178*(4), 1301–1307.

(21) Dhar, S. N.; Desai, C. F. Sb2Te3 and In0.2Sb1.8Te3: a comparative study of thermoelectric and related properties. *Philos. Mag. Lett.* **2002**, *82*(10), 581–587.

(22) Talapin, D. V.; Murray, C. B. PbSe nanocrystal solids for n- and p-channel thin film field-effect transistors. *Science* **2005**, *310*(5745), 86–89.

(23) Zhou, W.; Zhu, J.; Li, D.; Hng, H. H.; Boey, F. Y. C.; Ma, J.; Zhang, H.; Yan, Q. Binary-Phased Nanoparticles for Enhanced Thermoelectric Properties. *Adv. Mater.* **2009**, *21*(31), 3196–3200.

(24) Chen, G.; Hui, P. Pulsed photothermal modeling of composite samples based on transmission-line theory of heat conduction. *Thin Solid Films* **1999**, *339*(1−2), 58–67.

(25) Zhao, Y. M.; Chen, G.; Wang, S. Z.; Yoon, S. F. In *Thermal characterization of GaAsN thin films by pulsed photothermal reflectance technique*; Symposium on Nanoscale Imaging and Characterization of Materials, Singapore, Singapore, Dec 07−12, 2003; Yeadon, M.; Gong, H., Boothroyd, C. B., Eds.; World Scientific Publ Co Pte Ltd: Singapore, Singapore, 2003; pp 781−787.
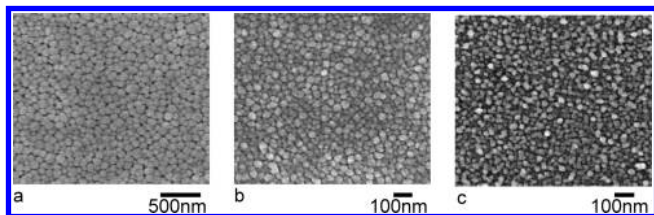
Figure 1. SEM images of Sb_2Te_3 nanoparticles obtained at (a) $d_{sub}=20$ cm, (b) 25 cm and (c) 30 cm, respectively.

The thermal conductivity of a 20 nm nanoparticle thin film was measured by pulsed photothermal reflectance (PPR).[24−26]

For the PPR technique, the measurement on film samples is carried out in the perpendicular direction to the surface as previously reported.[24] Before the measurement, the thin film sample, deposited on high-resistivity silicon substrate, is coated with a gold film layer of 1 μm thickness. Gold is preferred as a light absorption element because it is not susceptible to oxidation at room temperature and can reflect light differently at different wavelengths. The experiment begins with the gold film irradiated by a Nd:YAG laser pulse with a pulse width (full width at half-maximum, fwhm) of 8 ns, spot size of 3 mm, pulse energy of 30.3 μJ, and frequency of 10 Hz. Immediately after the laser pulse excitation, the sample's surface temperature rises sharply and then slowly relaxes to room temperature.[27] Estimated maximum surface temperature excursion is about 31 K, and the relaxation time is governed by the thermal properties of the underlying films. To obtain the temperature excursion profile, a focused continuous He−Ne probe laser is reflected from the gold film surface and a fast speed photodetector is used to capture the reflected light signal. Since the reflectivity is inversely related to the surface temperature, by inverting the acquired signal a temperature excursion profile can be obtained. The system was calibrated by measuring the thermal conductivity of silicon dioxide film. After conducting the experiment for the Au/Sb_2Te_3 nanostructures/Si structure, the temperature profile is curve fitted using the three-layer heat conduction model in which silicon substrate is modeled as an infinite medium.

Results and Discussion

A typical synthesis is carried out by placing two crucibles containing Te powder and Sb powder, respectively, in the center of the quartz tube that is heated at 853 K under continuous Ar/H_2 gas flow to transfer the Sb and Te vapors to be deposited onto glass substrates set in the downstream positions. Figure 1 shows the SEM images of the as-prepared nanoparticles by the vapor transport growth process. Analysis on the SEM images reveals that the average particle size of the films is highly dependent on the substrate position/temperature. Films with average particle sizes of 100, 50, and 20 nm were obtained on substrates placed at distances of $d_{sub} = 20$, 25, and 30 cm away from center of the furnace with substrate temperatures of 74, 40, and 36 °C, respectively. The substrate temperature is judged from the temperature profile of the

(26) Zhao, Y. M.; Chen, G.; Wang, S. Z.; Yoon, S. F. Thermal characterization of gallium arsenic nitride epilayer on gallium arsenide substrate using pulsed photothermal reflectance technique. *Thin Solid Films* **2004**, *450*(2), 352–356.

(27) Hay, B.; Filtz, J. R.; Hameury, J.; Davee, G.; Rongione, L.; Enouf, O. Thermal-Diffusivity Measurement of Ceramic Coatings at High Temperature using "Front-Face" and "Rear-Face" Laser Flash Methods. *Int. J. Thermophys.* **2009**, *30*(4), 1270–1282.
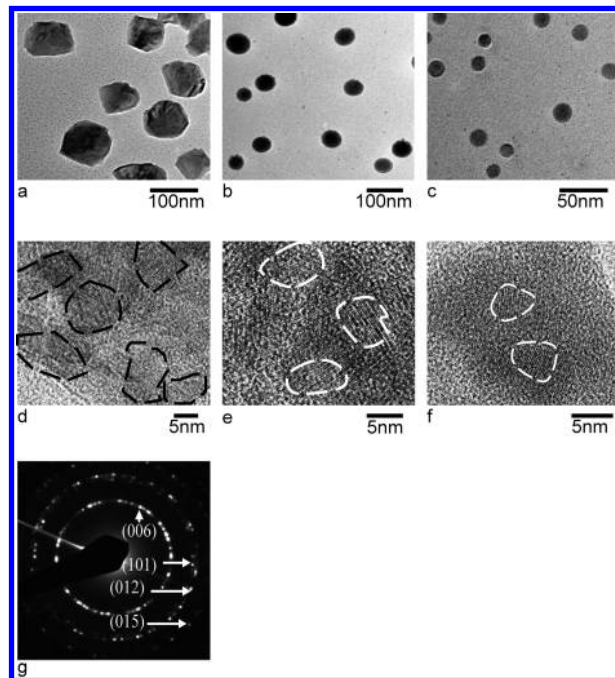
Figure 2. TEM images of Sb_2Te_3 nanoparticles obtained at (a) $d_{sub} = 20$ cm, (b) 25 cm and (c) 30 cm, respectively. HRTEM micrographs Sb_2Te_3 nanoparticles obtained at (d) $d_{sub} = 20$ cm, (e) 25 cm and (f) 30 cm, respectively, which show the polycrystalline nature of the nanoparticles. (g) SAED pattern of Sb_2Te_3 nanoparticles obtained at $d_{sub} = 30$ cm.

furnace at 853 K (see Supporting Information Figure S1). These nanoparticles show moderate size distribution (see Supporting Information Figure S2) as confirmed by the analysis of atomic force microscopy images (see Supporting Information Figure S3) and closely packed onto the substrates. Further increasing d_{sub} to 36 cm leads to formation of a particle film with even smaller average particle size, e.g. ~10 nm (see Supporting Information Figure S4). However, due to the slow growth rate, it requires a very long growth time, e.g. >6 h, to form a relatively continuous film with a thickness of ~150 nm. The Sb_2Te_3 nanoparticle films on the glass substrates were dipped into ethanol solution and subjected to sonication for TEM sample preparation. The resulting solution was drop cast onto Cu grids for TEM observation. Energy dispersive X-ray (EDX) analysis (see Supporting Information Figure S5) confirms that the ratio of Sb:Te is close to 2:3. Here, the carbon peak is mainly from the carbon film in the Cu grid. TEM images (Figure 2a−c and Supporting Information Figure S6b) reveal the faceting of 100 nm particle samples while samples of other sizes are relatively spherical. High resolution TEM (HRTEM) images (Figure 2d−f) indicate the polycrystalline nature of the nanoparticles. Selected area electron diffraction (SAED) pattern (Figure 2g) on the nanoparticle films exhibits rings corresponding to the rhombohedral Sb_2Te_3.

To investigate the crystal structure as well as estimate the size of the grains of the samples, X-ray diffraction (XRD) studies were carried out. The XRD patterns (Figure 3a) obtained for the as-prepared particle films confirm the existence of only the rhombohedral Sb_2Te_3 phase (JCPDS-ICDD card 15-0874), which is consistent with the SAED analysis (see Figure 2g) in TEM characterization.
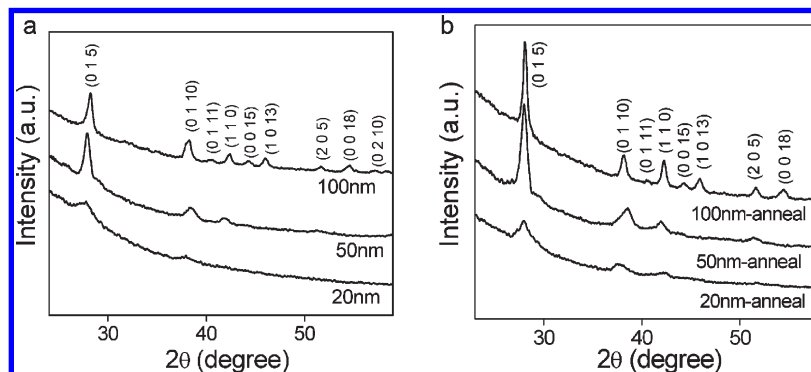
Figure 3. XRD patterns obtained from the different sized Sb_2Te_3 nanoparticles: (a) as-grown and (b) annealed at 523 K for 60 min.

Based on the analysis of the full width at half-maximum using the Scherrer equation,[28] the grain sizes are estimated to be about 6, 11, 15 nm for the 20, 50 and 100 nm particle films respectively. The result is consistent with the HRTEM observations. Here, it is noticed that the grain size of the samples is much smaller than that of Sb_2Te_3 nanocrystals made by wet-chemical approaches[29] and is smaller than/comparable to the de Broglie wavelength of Sb_2Te_3, e.g. 18 nm (estimated from the equation $\lambda_D = h/(2mk_BT)^{1/2}$),[30,31] which is important to induce the quantum size effect.[5] Actually, based on our previous experiments,[32] Sb or its compound nanoparticles are very difficult to synthesize with uniform shape and small size, e.g. < 20 nm, mainly due to lack of effective capping ligands interacting effectively with Sb. We also annealed the samples at 523 K for 60 min in H_2/Ar atmosphere, which is a useful process to improve the electrical conductivity. It is noted that grain coarsening is not obvious as suggested from the analysis of the peak width of the XRD patterns of the annealed samples, e.g. 6, 13, and 19 nm are obtained for the annealed 20, 50 and 100 nm particle films respectively (Figure 3b and Supporting Information Figure S6a−c). However, partial agglomeration of particles is observed in all three types of samples after such annealing process (see Supporting Information Figure S7a−c).

The formation of the Sb_2Te_3 nanoparticles is thought to be related to the island growth mode (Stranski−Krastanov growth mode)[33,34] of films due to the fast nucleation

process. In some cases, such growth may require epitaxial lattice mismatch between the substrates and the growth species, e.g. Ge on Si (100) surface.[33] Sb_2Te_3 in this growth process is not necessarily epitaxially attached to the glass substrates. The heterogeneous nucleation process and the fast nucleation rate are the keys to initiate the growth of these nanoparticles. Normally, slow nucleation and fast surface diffusion lead to single crystal film growth while fast nucleation leads to island growth.[35] The mass influx in this vapor transport growth is very high as compared to other typical thin film deposition techniques, e.g. sputtering or pulse laser deposition (PLD), thus it is helpful to incur fast nucleation while the diffusion of atom on glass may be slow enough to promote the nanoparticle film growth. We noticed that the surface of the substrate is a very important parameter in controlling the particle film growth. For example if Cu-coated Si substrates are used, the resulting films are composed of nonuniform continuous clusters. The particle size control was achieved by varying the precursor vapor pressure and substrate temperature. For a constant Ar/H_2 gas flow rate, smaller sized particles are deposited at longer d_{sub}. This is mainly due to (1) the lower substrate temperature that causes faster nucleation process[36] and (2) the lower precursor vapor pressure that slows down the growth process. However, the growth rates are lower at longer d_{sub}. It is noted that, for the same growth time of ∼60 min, the thickness of the particle film obtained at $d_{sub} = 20$ cm is > 1 μm, while for the particle film obtained at $d_{sub} = 30$ cm, the thickness is ∼200 nm.

The as-prepared Sb_2Te_3 particle films have smooth surfaces, and the thicknesses are highly uniform (see Supporting Information Figure S8a,b). This means that they can be used directly for electrical and thermal electrical characterization without further processing. The four-probe resistivity measurements in the temperature range of 323−600 K performed in the commercial ZEM 3 system reveal that the three types of films of different particle size have low electrical resistivity in the range of 10^{-4} Ω m (see Figure 4a). For thermoelectric semiconductors, low electrical resistivity is essential to

(28) Zhang, Z.; Zhou, F.; Lavernia, E. J. On the analysis of grain size in bulk nanocrystalline materials via X-ray diffraction. *Metall. Mater. Trans. A* **2003**, *34A*(6), 1349–1355.
(29) Shi, W. D.; Zhou, F.; Zhou, L.; Song, S. Y.; Yang, J. H.; Zhang, H. J. Hydrothermal synthesis and thermoelectric transport properties of impurity-free antimony telluride hexagonal nanoplates. *Adv. Mater.* **2008**, *20*(10), 1892–1897.
(30) Frumar, M.; Wagner, T.; Hrdlicka, M.; Frumarova, B.; Nemec, P. Non-volatile phase change memory materials and their induced changes. In *Plasmon Data Systems*; Cambridge, 2005.
(31) Wang, G. F.; Cagin, T. Investigation of effective mass of carriers in Bi2Te3Sb2Te3 superlattices via electronic structure studies on its component crystals. *Appl. Phys. Lett.* **2006**, *89*(15), 3.
(32) Yan, Q. Y.; Kim, T.; Purkayastha, A.; Ganesan, P. G.; Shima, M.; Ramanath, G. Enhanced chemical ordering and coercivity in FePt alloy nanoparticles by Sb-doping. *Adv. Mater.* **2005**, *17*(18), 2233–2237.
(33) Ross, F. M.; Tersoff, J.; Tromp, R. M. Coarsening of self-assembled Ge quantum dots on Si(001). *Phys. Rev. Lett.* **1998**, *80*(5), 984–987.
(34) Mo, Y. W.; Savage, D. E.; Swartzentruber, B. S.; Lagally, M. G. Kinetic pathway in Stranski-Krastanov growth of Ge on Si(001). *Phys. Rev. Lett.* **1990**, *65*(8), 1020–1023.
(35) Huang, H. C.; Gilmer, G. H.; de la Rubia, T. D. An atomistic simulator for thin film deposition in three dimensions. *J. Appl. Phys.* **1998**, *84*(7), 3636–3649.
(36) Surgers, C.; Strunk, C.; Lohneysen, H. Effect of substrate-temperature on the microstructure of thin niobium films. *Thin Solid Films* **1994**, *239*(1), 51–56.
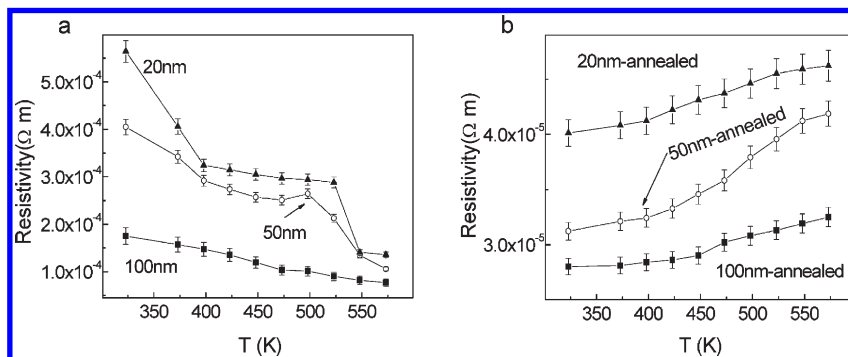
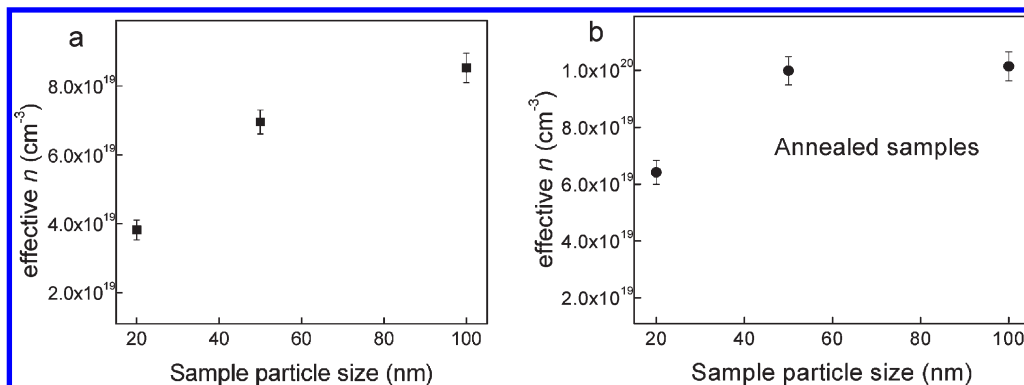**Figure 4.** Electrical resistivity of (a) as-grown and (b) annealed Sb_2Te_3 nanoparticles.

Figure 5. Room-temperature effective charge carrier concentration, n, of (a) as-prepared and (b) annealed Sb_2Te_3 samples with different particle sizes.

achieve high ZT values. For all three types of samples, the electrical resistivity decreases with temperature. Although this trend indicates a typical semiconductor behavior,[37] other factors may also affect the electrical resistivity of these samples, e.g. the annealing effect at higher measuring temperature leads to partial agglomeration and hence enhances the contact between the particles, which may also increase the electrical conductance. Thus, the measurement on the annealed samples is used to assess the intrinsic trend of the electrical conductance vs temperature. The enhanced contact between the particles in the annealed samples is evidenced from the SEM observations (see Supporting Information Figure S7a−c), and no obvious grain coarsening is observed as indicated by the XRD results (see Figure 3b). The electrical resistivity of the annealed samples shows improved values (see Figure 4b) as compared to their corresponding as-prepared ones. In addition, their values increase at higher temperatures, which is expected in metals or heavily doped semiconductors.[38] Here, we note that these electric resistivity values are lower than those of TE nanocrystals obtained by wet chemical process,[29] which is mainly a benefit from clean surface without capping of insulating ligands. For both the as-prepared and the annealed samples, the lower electrical resistivity shown in

the larger sized particle films is anticipated as the quantum size effect increases the band gap,[7] E_g, of the semiconductor particles.[5] The UV absorption spectra (see Supporting Information Figure S9) reveal that the onset of the threshold of absorption curve shows a blue shift for 20 nm Sb_2Te_3 nanoparticles as compared to that of 50 and 100 nm samples, which suggests the larger band gap value and is consistent with the results of the electrical resistivity measurements.

The effective charge carrier concentration, n, at room temperature has been investigated by using a Hall Effect measurement system (see Figure 5). For as-prepared samples, the effective charge carrier concentration[39] is in the range $3-8 \times 10^{19}$ cm^{-3}, which is ideal to achieve optimized ZT values.[40] The effective charge carrier concentration increases slightly, e.g. to $6-10 \times 10^{19}$ cm^{-3}, after annealing at 523 K for 60 min for all three types of samples. The higher effective charge carrier concentration obtained in larger sized particle films is expected as increasing the band gap due to quantum confinement may decrease the value of n.[7] Based on the charge carrier concentration data, we can estimate the effective hole mobility, μ, of the particle films using $\sigma = ne\mu$ (see Supporting Information Figure S10a,b). The estimated effective hole mobility of the samples increases by 5−7 times after the heat treatment, which is also

(37) Nagao, Y.; Terasaki, I.; Nakano, T. Dielectric constant and ac conductivity of the layered cobalt oxide Bi2Sr2CoO6+delta: A possible metal-dielectric composite made by self-organization of Co2+ and Co3+ ions. *Phys. Rev. B* **2007**, *76* (14).
(38) Brown, S. R.; Toberer, E. S.; Ikeda, T.; Cox, C. A.; Gascoin, F.; Kauzlarich, S. M.; Snyder, G. J. Improved thermoelectric performance in Yb14Mn1-xZnxSb11 by the reduction of spin-disorder scattering. *Chem. Mater.* **2008**, *20*(10), 3412–3419.

(39) Muthukumarasamy, N.; Balasundaraprabhu, R.; Jayakumar, S.; Kannan, M. D. Electrical conduction studies of hot wall deposited CdSexTe1-x thin films. *Sol. Energy Mater. Sol. Cells* **2008**, *92*(8), 851–856.
(40) Snyder, G. J.; Toberer, E. S. Complex thermoelectric materials. *Nat. Mater.* **2008**, *7*(2), 105–114.
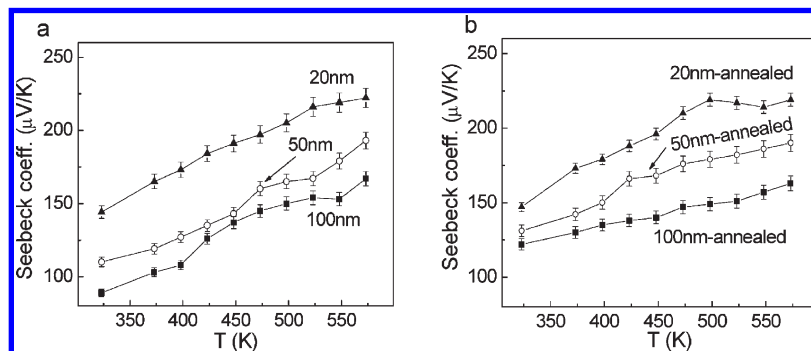
Figure 6. Seebeck coefficients of (a) as-grown and (b) annealed Sb_2Te_3 nanoparticles.
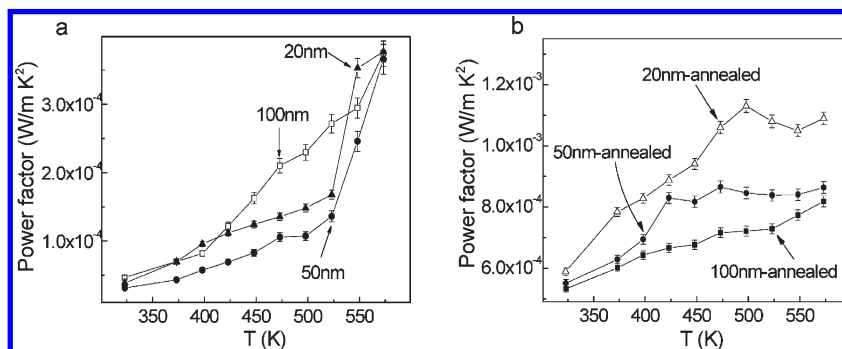

Figure 7. Power factors of (a) as-grown and (b) annealed Sb_2Te_3 nanoparticles.

in line with the increased electrical conductance. This suggests that enhanced contact among the particles after annealing can effectively reduce the interface scattering of the charge carriers.

Thermoelectric characterization with the ZEM 3 system shows that all three sized Sb_2Te_3 particle films are p-type with high maximum Seebeck coefficients, e.g. $> 200 \, \mu V/K$, $> 180 \, \mu V/K$, and $> 160 \, \mu V/K$ for 20 nm, 50 nm and 100 nm particle films, respectively (see Figure 6a). These values are higher than that of bulk Sb_2Te_3 crystals (79 $\mu V/K$) with similar charge carrier concentrations[20,21] and that of Sb_2Te_3 thin film.[41] If the Sb_2Te_3 nanocrystal size is increased by decreasing the d_{sub}, the Seebeck coefficient is reduced to $60-95 \, \mu V/K$ in the same temperature range (see Supporting Information Figure S11) while the Sb_2Te_3 are single-crystal nanoplates with a diameter of $2-3 \, \mu m$ and a thickness of $80-200$ nm. The enhanced Seebeck coefficient, S, in smaller particles is thought to be possibly related to the quantum confinement effect that increases the difference between the Fermi level and the average mobile carrier energy,[7] or to be related to the energy filtering effect due to the charge carrier trapped in the grain boundaries regions.[42] All three sized particle films show increased S at higher temperature range. For heavily doped semiconductor or metal, the electron contribution to S is proportional to the

absolute temperature.[43] The values of S for the annealed samples are comparable to those of the as-prepared ones (see Figure 6b), although their electrical resistivities are significantly lower.

The plots of power factor (see Figure 7) defined as $S^2\sigma$ of the as-prepared samples show values $> 3 \times 10^{-4} \, W/mK^2$ at $T > 550$ K. The power factors for the annealed samples are significantly improved by $2-3$ times. A maximum power factor $> 1.1 \times 10^{-3} \, W/mK^2$ was measured in the 20 nm particle films at $T = 500$ K. The smaller sized particle films show higher power factor mainly due to the contribution of their higher values of Seebeck coefficients.

The measurement of κ for nanostructures or even thin films is very difficult[10,44] due to the small feature size. Here, we carried out the pulsed photothermal reflectance (PPR)[24,25] process to evaluate the thermal conductivity of the samples. Here, we noted that the PPR measurements can only test the thermal conductivity along the normal of the particle film surface while the previous discussion on the Seebeck and electrical conductivity is along the surface of the samples. Although these nanoparticle-assembled films are expected to be isotropic because of their unique build-up structures, we cannot claim ZT values based on these measurements. For the PPR method as discussed in detail in the Experimental Section (also see Supporting Information Figure S12), the thermal conductivity, κ, is obtained by curve fitting the time dependence surface temperature profile of the Au film coated sample with the three-layer heat conduction model

(41) Rajasekar, K.; Kungumadevi, L.; Subbarayan, A.; Sathyamoorthy, R. Thermal sensors based on Sb2Te3 and (Sb2Te3)(70)(Bi2Te3)(30) thin films. *Ionics* **2008**, *14*(1), 69–72.

(42) Martin, J.; Wang, L.; Chen, L.; Nolas, G. S. Enhanced Seebeck coefficient through energy-barrier scattering in PbTe nanocomposites. *Phys. Rev. B* **2009**, *79*(11), 5.

(43) Rowe, D. M. *CRC handbook of thermoelectrics*; CRC Press: London, New York, Washington, DC, 1995.

(44) Boukai, A. I.; Bunimovich, Y.; Tahir-Kheli, J.; Yu, J. K.; Goddard, W. A.; Heath, J. R. Silicon nanowires as efficient thermoelectric materials. *Nature* **2008**, *451*, 168–171.

Table 1. Room Temperature Thermal Conductivity (W/mK) of Sb₂Te₃ Nanoparticle Samples Determined by Pulsed Photothermal Reflectance

as-prepared samples			annealed samples		
100 nm	50 nm	20 nm	100 nm	50 nm	20 nm
0.5	0.38	0.23	0.78	0.55	0.33

(see Supporting Information Figure S13a−f). Although the PPR measurements have the advantages that they do not require the known values of density and specific heat of the samples, only room-temperature thermal conductivity of as-prepared and annealed samples can be obtained (see Table 1 and Supporting Information Figure S13a−f) due to the limit of instrumental setup. The PPR measurement indicates that the 20 nm Sb₂Te₃ nanoparticle films show much reduced values of κ at room temperature, e.g. 0.23 W/mK for as-prepared samples and 0.33 W/mK for annealed samples, which is much lower than that reported for compact bulk Sb₂Te₃, e.g. ~1 W/mK.[45] The values of the thermal conductivity for Sb₂Te₃ samples with different particles sizes, e.g. 0.2−0.5 W/mK for as-prepared particles and 0.3−0.8 W/mK for annealed particles, are comparable to those recently reported values for Bi₂Te₃ nanoparticles.[46,47] Here, the estimated carrier thermal conductivity is not high,

e.g 0.012−0.04 W/mK for as-prepared samples and 0.17−0.26 W/mK for annealed samples, using Wiedemann−Franz's law,[48,49] e.g. $\kappa_{carrier} = LT/\rho$, where L is the Lorenz number, e.g. 2.45×10^{-8} V² K⁻², ρ is the electrical resistivity, and T is the temperature in kelvins. Preparation of these Sb₂Te₃ nanoparticles in large scale can further enable accurate thermal conductivity measurements by laser flash process[27] to enable estimation of the ZT values, which is ongoing now. Also, further enhanced thermoelectric properties can be expected by applying this approach to prepare nanoparticles of other material systems with proven higher ZT values, e.g. BiSbTe[4,8] or AgPbSbTe.[9]

In summary, we have demonstrated a new facile process to grow Sb₂Te₃ nanoparticle films with controlled particle size using a catalyst-free vapor transport growth technique. Such a growth process allows the realization of nanocrystal films with tunable crystal size, e.g. 5−15 nm, comparable to the de Broglie wavelength of Sb₂Te₃. The enhancement of the Seebeck coefficients has been demonstrated in these nanoparticle films as compared to that of bulk Sb₂Te₃ with similar charge carrier concentration. Meanwhile, these particle films show high electrical conductivities due to the clean particle surfaces. The PPR measurements at room temperature suggest that these nanoparticle films show much reduced thermal conductivity as compared to that of bulk Sb₂Te₃. Thus, this approach demonstrates a promising route to achieve new types of highly efficient TE semiconductors.

Supporting Information Available: Temperature profile of the furnace, morphology and the estimated mobility of the samples, detail of PPR measurement (PDF). This material is available free of charge via the Internet at http://pubs.acs.org.

(45) Wang, W.; Yan, X.; Poudel, B.; Ma, Y.; Hao, Q.; Yang, J.; Chen, G.; Ren, Z. Chemical synthesis of anisotropic nanocrystalline Sb2Te3 and low thermal conductivity of the compacted dense bulk. *J. Nanosci. Nanotechnol.* **2008**, *8*(1), 452–456.
(46) Scheele, M.; Oeschler, N.; Meier, K.; Kornowski, A.; Klinke, C.; Weller, H. Synthesis and Thermoelectric Characterization of Bi2Te3 Nanoparticles. *Adv. Funct. Mater.* **2009**, *19*(21), 3476–3483.
(47) Dirmyer, M. R.; Martin, J.; Nolas, G. S.; Sen, A.; Badding, J. V. Thermal and Electrical Conductivity of Size-Tuned Bismuth Telluride Nanoparticles. *Small* **2009**, *5*(8), 933–937.
(48) Yang, L.; Hng, H. H.; Li, D.; Yan, Q. Y.; Ma, J.; Zhu, T. J.; Zhao, X. B.; Huang, H., Thermoelectric properties of p-type CoSb3 nanocomposites with dispersed CoSb3 nanoparticles. J. Appl. Phys. **2009**, *106*, (1).
(49) Li, D.; Yang, K.; Hng, H. H.; Yan, Q. Y.; Ma, J.; Zhu, T. J.; Zhao, X. B., Synthesis and high temperature thermoelectric properties of calcium and cerium double-filled skutterudites Ca0.1CexCo4Sb12. J. Phys. D: Appl. Phys. **2009**, *42* (10).